The Rag2 Il2rb Dmd mouse: a novel dystrophic and immunodeficient model to assess innovating therapeutic strategies for muscular dystrophies.

Denis Vallese, Elisa Negroni, Stéphanie Duguez, Arnaud Ferry, Capucine Trollet, Ahmed Aamiri, Christian A. J. Vosshenrich, Ernst-Martin Füchtbauer, James P Di Santo, Libero Vitiello, et al.

The *Rag2*$^{-}$*Il2rb*$^{-}$*Dmd*$^{-}$ Mouse: a Novel Dystrophic and Immunodeficient Model to Assess Innovating Therapeutic Strategies for Muscular Dystrophies

Denis Vallese[1–4], Elisa Negroni[1–3], Stéphanie Duguez[1–3], Arnaud Ferry[1–3], Capucine Trollet[1–3], Ahmed Aamiri[5], Christian AJ Vosshenrich[6,7], Ernst-Martin Füchtbauer[8], James P Di Santo[6,7], Libero Vitiello[4], Gillian Butler-Browne[1–3] and Vincent Mouly[1–3]

[1]*UPMC Université Pierre et Marie Curie (UPMC), UM76, Institut de Myologie, Paris, France;* [2]*INSERM U 974, Institut de Myologie, Paris, France;* [3]*CNRS UMR 7215, Institut de Myologie, Paris, France;* [4]*Department of Biology, University of Padova, Padova, Italy;* [5]*Laboratoire LBCM, Departement de Biologie, Faculté des Sciences, Université d'Agadir, Agadir, Morocco;* [6]*Innate Immunity Unit, Institut Pasteur, Paris, France;* [7]*Inserm U668, Paris, France;* [8]*Department of Molecular Biology and Genetics, Aarhus University, Aarhus, Denmark*

The development of innovative therapeutic strategies for muscular dystrophies, particularly cell-based approaches, is still a developing field. Although positive results have been obtained in animal models, they have rarely been confirmed in patients and resulted in very limited clinical improvements, suggesting some specificity in humans. These findings emphasized the need for an appropriate animal model (i.e., immunodeficient and dystrophic) to investigate *in vivo* the behavior of transplanted human myogenic stem cells. We report a new model, the *Rag2*$^{-}$*Il2rb*$^{-}$*Dmd*$^{-}$ mouse, which lacks T, B, and NK cells, and also carries a mutant Dmd allele that prevents the production of any dystrophin isoform. The dystrophic features of this new model are comparable with those of the classically used *mdx* mouse, but with the total absence of any revertant dystrophin positive fiber. We show that *Rag2*$^{-}$*Il2rb*$^{-}$*Dmd*$^{-}$ mice allow long-term xenografts of human myogenic cells. Altogether, our findings indicate that the *Rag2*$^{-}$*Il2rb*$^{-}$*Dmd*$^{-}$ mouse represents an ideal model to gain further insights into the behavior of human myogenic stem cells in a dystrophic context, and can be used to assess innovative therapeutic strategies for muscular dystrophies.

Received 14 May 2013; accepted 25 July 2013; advance online publication 24 September 2013. doi:10.1038/mt.2013.186

INTRODUCTION

Muscular dystrophies are a heterogeneous group of inherited disorders characterized by progressive muscle weakness and wasting. The most severe form, Duchenne muscular dystrophy (DMD), affects 1:5,000 live male births and is caused by mutations in the dystrophin gene.[1] Dystrophin is a very large protein that is part of a complex linking the extracellular matrix and the sarcolemma to the cytoskeleton and sarcomeres; its absence causes permanent fragility and leakiness of the sarcolemma, leading to Ca^{2+} influx and disruption of the muscle fibers resulting in repeated cycles of degeneration–regeneration.[2] These cycles will gradually deplete the endogenous pool of myogenic precursor cells that eventually can no longer compensate for the ongoing fiber disruption.[3]

The availability of reliable animal models is essential for evaluating therapeutic approaches in preclinical studies for such muscular dystrophies. Many animal models of muscular dystrophies, either naturally occurring or genetically engineered, have been described in the past.[4] The first to be reported – and the most widely used – is the *mdx* mouse with a point mutation resulting in a premature stop codon in exon 23 of the dystrophin gene (Dmd^{mdx}).[5,6] However, *mdx* muscles show the presence of a variable number of dystrophin-positive "revertant" fibers, whose number increases with age rising up to 200 or more dystrophin-positive fibers in the quadriceps of adult *mdx* mice.[7] Although this number rarely exceeds 5% of the total number of fibers, their presence can hinder the precise assessment of a dystrophin-restoring therapeutic approach. The *mdx* mouse has been widely used to assess different kinds of therapeutic approaches, including pharmacological,[8] gene,[9] or cell-based therapies.[10] The latter has been pioneered by the group of T Partridge and colleagues as early as 1978.[11] Since then, it has been further explored by many research groups using transplanted dystrophin-expressing myoblasts, either autologous and genetically engineered or derived from a healthy donor. As a result of these promising results, a number of clinical trials were initiated in the 1990's on DMD patients, mainly using allogenic transplantation of myoblasts, but despite the promising results observed in *mdx* mice, they failed to bring significant therapeutic benefits to the patients. In fact, even though no severe side effects were reported, in the best-case scenario only short-lasting dystrophin expression and a slight improvement in muscle strength was achieved, see[10] for a review. The discrepancy of the results obtained in mouse and in clinical trials emphasized the importance of developing better animal models (i.e., immunodeficient and dystrophic) to investigate *in vivo* the limiting parameters, taking into account the specific requirements and behavior of human myogenic progenitors (e.g., myoblasts, mesoangioblasts, $CD133^{+}$, $ALDH^{+}$, and so on, see[10] for a review).

Correspondence: Vincent Mouly, Thérapie des Maladies du Muscle Strié/Institut de Myologie, UM76 – UPMC Université Paris 6/U974 – Inserm/UMR7215 – CNRS, 47, Bld de l'hôpital – G.H. Pitié-Salpétrière – Bâtiment Babinski, 75651, Paris, France. E-mail: vincent.mouly@upmc.fr

Currently available immunodeficient dystrophic mouse models used to assess the success of human cell transplantation present some drawbacks: maintenance of the colony, which may be hampered by excessive immunodeficiency, or rejection of the transplanted cells due to unstable immunodeficiency. The most widely used strains are the *nude/mdx* (*Foxn1*$^{-}$*Dmd*^{mdx}) and the *scid/mdx* (*Prkdc*$^{-}$*Dmd*^{mdx}) mice; the former is only partially deficient, since it lacks only T-cells due to thymic dysgenesis, whereas the latter has a defect in both T- and B-cell development.[12,13] Importantly, both strains retain NK-cell activity, which can give rise to an immune response against the grafted cells. Moreover, as *scid* mice have a 'leaky' phenotype, they show the spontaneous production of functional lymphocytes with age and increased propensity for thymic lymphoma development, both of which limits long-term graft survival.[14] These limitations are in addition to the problem of revertant fibers formation in the *mdx* background.

To avoid the possibility of immune-mediated rejection of human xenografts, mice that have stable and complete lymphoid deficiencies have been developed. These are based on mice with combined mutations in the recombinase-activating gene 2 (Rag2, which blocks T- and B-cell development)[15] and in cytokine receptors, such as the β or γ subunits of the IL-2 receptor gene (*Il2rb* or *Il2rg*) that block NK cell development. As such, *Rag2*$^{-}$*Il2rb*$^{-}$ and *Rag2*$^{-}$*Il2rg*$^{-}$ mice[16,17] are completely alymphoid and lack B, T, and NK cells. These mice have proved useful for the study of human myoblast xenografts but require recipient mouse muscle conditioning (cryolesion, toxins) in order to create a 'niche' for subsequent human muscle fiber development.

In this report, we have introduced a nonrevertant mutant dystrophin (*Dmd*$^{mdx\text{-}\beta geo}$; harboring an insertion of ROSAβgeo vector in the 3′ of exon 63 of the murine Dmd gene) onto the *Rag2*$^{-}$*Il2rb*$^{-}$ background. In the *Dmd*$^{mdx\text{-}\beta geo}$ mouse, βgeo is spliced to dystrophin exon 63, replacing the sequences encoding the cysteine-rich domain and the C-terminus, resulting in a mutation that affects all presently known dystrophin isoforms and prevents any dystrophin re-expression and thus completely eliminates the problem of revertant fiber formation.[18] This new mouse model (*Rag2*$^{-}$*Il2rb*$^{-}$*Dmd*$^{-}$) is therefore highly and stably immunodeficient and cannot form revertant dystrophin fibers.

This study presents a full characterization of the muscle phenotype of this new immunodeficient and dystrophic model. As reference, we choose the most commonly used dystrophic model, the *mdx* mouse. We show that *Rag2*$^{-}$*Il2rb*$^{-}$*Dmd*$^{-}$ mice display characteristic dystrophic features: compensatory hypertrophy of hind limb muscles, elevated creatine kinase serum levels, intense muscle regeneration, and decreased muscle strength. Importantly, we also performed xenotransplantation of human myoblasts in this model, showing that *Rag2*$^{-}$*Il2rb*$^{-}$*Dmd*$^{-}$ mice are perfectly suited to investigate long-term xenografts, with maturation of donor-derived muscle fibers, thus making this model an ideal candidate to gain further insights into the behavior of human stem cells, the feasibility of innovative cell and gene therapeutic strategies, and the multiple consequences of restoring dystrophin in a dystrophic context.

RESULTS

We measured whole body weight, tibialis anterior (TA), and gastrocnemius muscle weights of *Rag2*$^{-}$*Il2rb*$^{-}$*Dmd*$^{-}$, *mdx*, and *wt* age-matched males mice over time (**Table 1**). Global body weight was not statistically different between *Rag2*$^{-}$*Il2rb*$^{-}$*Dmd*$^{-}$, *mdx*, and *wt* strains; however, while TA and gastrocnemius muscle weights were comparable between *Rag2*$^{-}$*Il2rb*$^{-}$*Dmd*$^{-}$ and *mdx*, they were significantly heavier than *wt* muscles.

In order to assess the kinetics of the cycles of degeneration/regeneration in the *Rag2*$^{-}$*Il2rb*$^{-}$*Dmd*$^{-}$ mice, we measured serum creatine kinase (CK) levels as an index of ongoing muscle membrane instability and evaluated the number of fibers with centrally located nuclei that already regenerated as well as the number of fibers expressing neonatal MyHC as a marker of ongoing regeneration. *Rag2*$^{-}$*Il2rb*$^{-}$*Dmd*$^{-}$ mice had high CK levels at all time points analyzed, with however some differences in the time course of CK levels between *Rag2*$^{-}$*Il2rb*$^{-}$*Dmd*$^{-}$ and *mdx* mice (**Figure 1a**). *Mdx* mice reached a maximum CK level at 8 weeks, whereas *Rag2*$^{-}$*Il2rb*$^{-}$*Dmd*$^{-}$ mice had CK values slightly lower than *mdx* until 24 weeks where it reached a maximum. The number of fibers with centrally located nuclei evaluated in TA muscles ranged from 35% at 4 weeks up to over 65% after 12 weeks, comparable with *mdx* TA muscles (**Figure 1b**). Neonatal MyHC-staining on TA sections

Table 1 Measurement of body and skeletal muscles weights of dystrophic and control mouse strains

	Body weight (g)			Muscle weight (mg)					
				TA			GAS		
	wt	*mdx*	*Rag2*$^{-}$*Il2rb*$^{-}$*Dmd*$^{-}$	*wt*	*mdx*	*Rag2*$^{-}$*Il2rb*$^{-}$*Dmd*$^{-}$	*wt*	*Mdx*	*Rag2*$^{-}$*Il2rb*$^{-}$*Dmd*$^{-}$
4 weeks	21.6 ± 1.0	16.4 ± 0.7	14.5 ± 0.9*,†††	34.9 ± 2.9	27.6 ± 1.4††	22.3 ± 2.0*,†††	88.7 ± 10.7	67.1 ± 3.0†	52.8 ± 7.1†
6 weeks	22.7 ± 0.3	21.9 ± 1.3	25.0 ± 1.4*,†	36.4 ± 3.3	44.9 ± 7.7	48.1 ± 2.9†	83.8 ± 2.0	103.6 ± 15.0†	108.3 ± 6.4*,†††
8 weeks	23.3 ± 2.2	26.3 ± 2.3	26.0 ± 1.8	47.4 ± 2.0	62.9 ± 1.2††	54.9 ± 6.4†	116.7 ± 15.2	143.9 ± 34.7	132.4 ± 14.1
12 weeks	25.7 ± 0.7	31.1 ± 1.6†††	32.9 ± 2.3†††	48.9 ± 4.4	73.8 ± 8.8††	75.2 ± 14.3††	128.6 ± 8.7	185.1 ± 16.7†††	136.1 ± 12.1†††
16 weeks	31.6 ± 2.6	32.5 ± 0.5	34.3 ± 0.6	52.2 ± 4.7	78.6 ± 9.7††	89.2 ± 4.4†††	120.2 ± 16.6	205.3 ± 12.9††	179.0 ± 33.4††
24 weeks	36.9 ± 4.7	34.4 ± 2.4	33.4 ± 2.3	52.9 ± 4.1	83.3 ± 6.1†††	79.8 ± 10.1†††	134.7 ± 13.1	199.7 ± 24.9††	147.9 ± 12.0††
43 weeks	27.3 ± 2.3	36.6 ± 2.3†	34.6 ± 3.9†	48.4 ± 6.7	93.1 ± 9.9††	83.9 ± 12.5††	123.0 ± 8.1	181.7 ± 22.1†	165.0 ± 23.2†

Body weights. Mean ± SEM are shown for each mouse model and for each age group. n = 3–6 per point. Differences between dystrophic strains are indicated as follow: $^{*}P < 0.05$, $^{***}P < 0.001$ compared with *mdx*, $^{\dagger}P < 0.05$, $^{\dagger\dagger}P < 0.01$, $^{\dagger\dagger\dagger}P < 0.001$ compared with *wt* control. *Muscle weights*. Mean ± SEM are shown for Tibialis anterior (TA) and Gastrocnemius (GAS) muscles, for male animals of each mouse model, and for each age group ($n \geq 3$). Differences between dystrophic strains are indicated as follow: $^{*}P < 0.05$, $^{***}P < 0.001$ compared with *mdx*, $^{\dagger}P < 0.05$, $^{\dagger\dagger}P < 0.01$, $^{\dagger\dagger\dagger}P < 0.001$ compared with *wt* control.

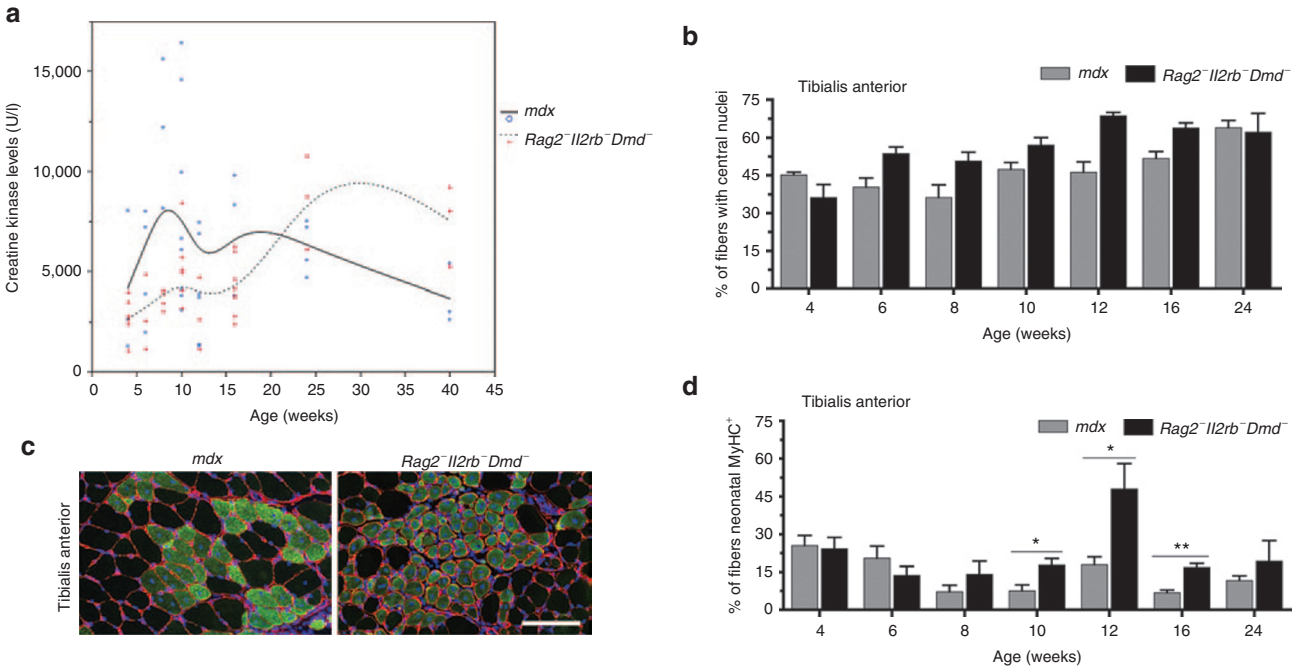

Figure 1 Evaluation of creatine kinase (CK) levels and chronology of regeneration. Time course representation of the CK serum levels of *Rag2*$^{-}$*Il2rb*$^{-}$*Dmd*$^{-}$ mice compared with *mdx* (**a**). Evaluation (**c**) and quantification (**b** and **d**) of the regeneration process in muscles of *Rag2*$^{-}$*Il2rb*$^{-}$*Dmd*$^{-}$ mice compared with *mdx*: muscle sections from 12-week-old mice stained for neonatal MyHC (green), laminin (red), and nuclei (blue). Numbers of fibers with central nuclei or expressing the neonatal MyHC protein are expressed as percentage of the total number of fibers; error bars are shown as mean ± SEM. $n = 3$–4 per time-point. *$P < 0.05$, **$P < 0.01$. Scale bar 200 µm.

(**Figure 1c**) confirmed a delayed degeneration/regeneration process in *Rag2*$^{-}$*Il2rb*$^{-}$*Dmd*$^{-}$ compared with *mdx* mice with a statistically significant increase in the number of regenerating fibers at 10, 12, and 16 weeks with a maximum at 12 weeks (**Figure 1d**).

We then assessed *Rag2*$^{-}$*Il2rb*$^{-}$*Dmd*$^{-}$ and *mdx* mice for absolute maximal force generation of the TA at 16 weeks and observed in both cases a 15% decrease compared with *wt* mice ($P < 0.05$, data not shown). Maximal force was then normalized for muscle weight to assess specific maximal force (**Figure 2a**), which clearly showed a significant force deficit in both dystrophic animal models (39 and 34% decrease for *mdx* and *Rag2*$^{-}$*Il2rb*$^{-}$*Dmd*$^{-}$, respectively, $P < 0.001$ in both cases). Following a series of lengthening contractions, we further confirmed that the TA muscles of both *mdx* and *Rag2*$^{-}$*Il2rb*$^{-}$*Dmd*$^{-}$ mice underwent a progressive and similar force drop, resulting in an overall force deficit of ~90% when normalized to the initial maximal force (**Figure 2b**). In contrast, the TA muscle of *wt* mice tolerated this level of contraction-induced muscle injury, decreasing by only 12%.

We next quantified the amount of connective tissue in TA and diaphragm muscles of *Rag2*$^{-}$*Il2rb*$^{-}$*Dmd*$^{-}$ mice by Sirius Red staining. In the TA, although we found an increase of inflammatory cells (neutrophils and macrophages) that correlates with the degeneration/regeneration processes (**Supplementary Figure S1**), the amount of connective tissue were below 10% at all time points (data not shown), whereas a high level of fibrosis was observed in the diaphragm at 43 weeks, a value similar to that observed in *mdx* mice (**Figure 2c**). This phenotype is not further aggravated with time, since the level of fibrosis quantified in the diaphragm at 43 weeks is not statistically different from that observed at 56 weeks.

By immunostaining, we confirmed that no revertant fibers were ever present in the *Rag2*$^{-}$*Il2rb*$^{-}$*Dmd*$^{-}$ mouse (**Figure 3a**), also when muscle sections were stained with an anti–n-terminal antibody (data not shown). We then investigated the efficacy of xenotransplantation of human primary myoblasts in TA muscles of *Rag2*$^{-}$*Il2rb*$^{-}$*Dmd*$^{-}$ *mouse*, as a proof of concept for this model to be used to assess the regenerative capacity of human cells in a dystrophic and immunodeficient environment. We performed intramuscular injections of 5×10^5 cells with and without cryodamage, in order to test the natural dystrophic environment versus enhanced degeneration. Immunohistochemical analysis of TA muscles 4 weeks after injection using human specific antibodies, revealed the presence of mature fibers in both conditions. A higher number of spectrin-positive fibers was obtained when the cryodamage was applied, but the difference was not statistically significant upon *t*-test (**Figure 3b**). It should be noted that all fibers expressing human spectrin that were analyzed were also positive for human dystrophin.

We also verified if newly formed human-derived muscle fibers were capable of expressing human dystrophin. Muscle sections were stained with antibody against human spectrin and lamin A/C, in order to identify human fibers and nuclei, and we then detected fibers expressing dystrophin with human specific antibodies (**Figure 4a**). To further assess the properties of dystrophin^{+} fibers, we checked the localization of the dystrophin-associated protein complex by immunostaining using human specific antibodies. β-dystroglycan and β-sarcoglycan were each observed at their proper location, the sarcolemma (**Figure 4b**). Importantly, we also verified whether injected human myoblasts could enter the satellite cell (SC) pool into the host tissue by staining muscle section with an antibody against Pax7. Human Pax7-positive cells were found between the

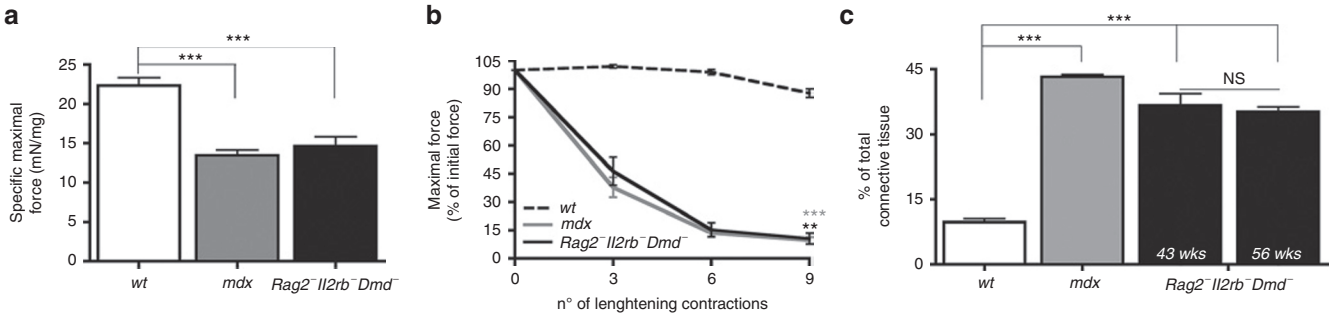

Figure 2 Measures of muscle force and analysis of fibrosis deposition. Tibialis anterior muscles of 16-week-old male *Rag2⁻Il2rb⁻Dmd⁻* mice were analyzed for their specific maximal force compared with *mdx* (**a**); muscles from male *wt* animals were used as age-matched controls. Dystrophic and control muscles were assessed for force drop following a series of nine lengthening contractions. The extent of force drop over successive lengthening contractions was measured and is presented as the percentage of the initial maximal force (**b**). Diaphragm muscle sections of 43-week-old *Rag2⁻Il2rb⁻Dmd⁻* and *mdx* mice were stained with Sirius Red to evaluate the fibrosis deposition, muscles from *wt* animals were used as age-matched controls. Total amount of connective tissue (endomysial plus perymisial) is expressed as percentage of the total muscle area (**c**). Error bars are shown as mean ± SEM. $n = 3–9$ *per group*. $^{**}P < 0.01$, $^{***}P < 0.001$ compared with *wt*.

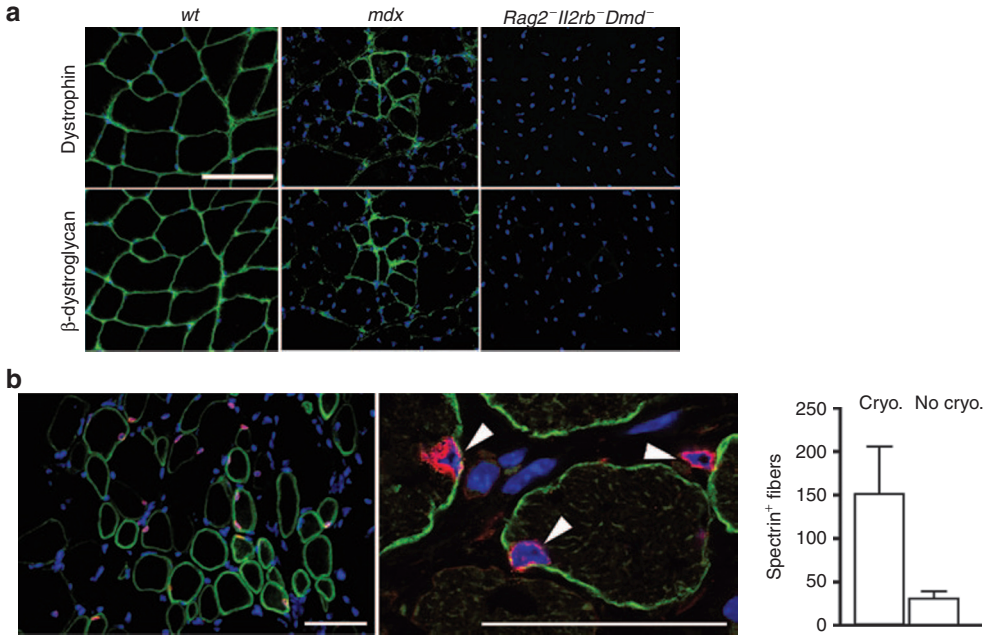

Figure 3 Proof of concept of human myoblast transplantation into the tibialis anterior of *Rag2⁻Il2rb⁻Dmd⁻* mice. Sections of TA muscle from *Rag2⁻Il2rb⁻Dmd⁻* and *mdx* mice were stained for dystrophin and β-dystroglycan (green) and nuclei (blue) to verify the presence of revertant fibers (**a**). At least three TAs from three different animals were analyzed. Human myoblasts contributed to the generation of new muscle fibers following injection into TAs of *Rag2⁻Il2rb⁻Dmd⁻* mice (**b**). Spectrin antibody (green) is used to identify human specific muscle fibers. Human nuclei are identified with a human-specific lamin A/C staining (red, white arrows in middle panel in **b**) among all nuclei (hoechst, blue), and are found either within human fibers or located in the interstitial space. Injection of human myoblast after cryodamage results in an higher number of Spectrin$^+$ fibers per cross sectional area (right panel, **b**). Error bars are shown as mean ± SEM. $n = 3$ per condition. Scale bar 100 µm in **a** and **b**.

sarcolemma and the basal lamina of human spectrin$^+$ muscle fibers (Figure 5d), and they represent 4.3% of the total donor nuclei when injected into cryodamaged TAs. Moreover, human lamin A/C$^+$ Pax7$^+$ SCs were also found within mouse muscle fibers, probably representing human nuclei that have been very recently integrated into the host's fibers (data not shown).

DISCUSSION

The field of therapeutic strategies for muscular dystrophies includes a very wide variety of approaches: pharmacological therapies, gene therapy, gene surgery, cell transplantation are different strategies – which can be used individually or in combination – that aim to replace, correct or repair the gene or transcript, or providing the missing protein, that are being developed to treat muscular dystrophies.

The variability of the results obtained in cell therapy clinical trials for skeletal muscle disorders in terms of clinical benefit for the patient, and the multiple therapeutic cell candidates that emerged in the past years – such as mesoangioblasts, CD133$^+$, ALDH$^+$, adipose-derived mesenchymal stem cells and so on (see[10,19,20] for review) – emphasize the urgent need to define a reliable animal model to assess and quantify the myogenic potential of these human myogenic stem cells within a dystrophic environment.

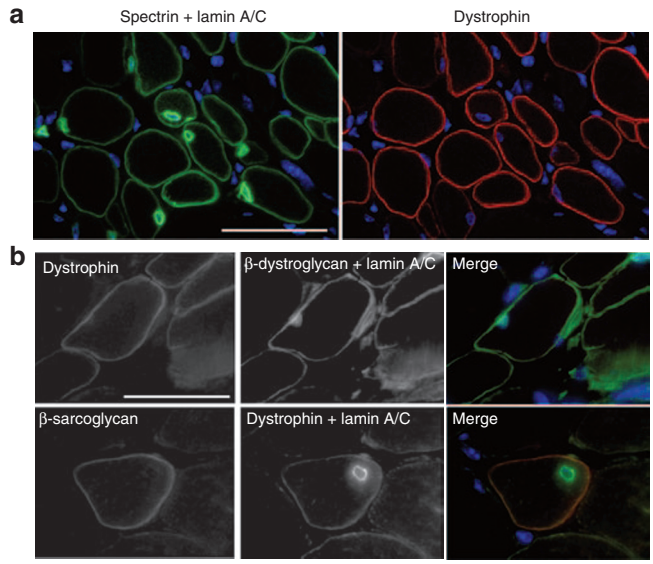

Figure 4 Restoration of the dystrophin-glycoprotein complex (DGC) by human transplanted cells. Human fibers, identified by human-specific antibodies against Spectrin and Lamin A/C (green), were also positive for human dystrophin (red, **a**). Human dystrophin^{+} fibers colocalize with β-dystroglycan (upper row, **b**). Human nuclei are identified with a human-specific lamin A/C staining (middle panel, upper row, **b**). In the lower row is shown the colocalization of dystrophin and β-sarcoglycan in human dystrophin^{+} fibers. Human nuclei are identified with a human-specific lamin A/C staining (middle panel). The colocalization of dystrophin and β-sarcoglycan was determined using human specific antibodies. All nuclei were counterstained using Hoechst (blue channel). Scale bar 100 µm in **a** and **b**.

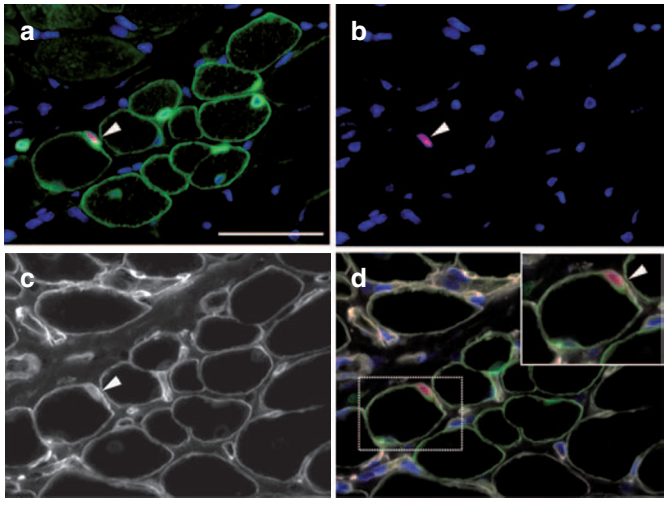

Figure 5 Transplanted human myoblasts enter the endogenous SC pool. Immunofluorescence analyses were used to visualize human lamin A/C and spectrin (**a**, green), Pax7 (**b**, red), and laminin (**c**, gray). Nuclei are counterstained with Hoechst. Human lamin A/C^{+} Pax7^{+} SCs were localized between spectrin and basal lamina (arrowhead), as shown in **d**. Inset: higher magnification picture showing a human SC located between Spectrin (green) and Laminin (gray). Scale bar = 50 µm.

Preclinical cell-therapy studies are usually limited to intramuscular or systemic injections of murine (or eventually canine) myogenic stem cells in mice, but very few studies take into account the specificity of human cells. *In vivo* evaluation of therapeutic approaches based on human cells will necessarily involve the use of immunodeficient animal models, capable of tolerating xenografts. Consequently, an appropriate animal model that would be a good host for injection of human cells into a dystrophic context is required. At present, three dystrophic immunodeficient mouse models have been described: the *nude/mdx*,[21,22] the *scid/mdx*[23] and the recently made *Rag2/mdx* mouse model.[24] All three murine models lack dystrophin but their immunodeficient phenotype is not complete, since the genetic mutations harbored by these mouse models do not affect the NK-cell activity.[15,25,26] This latter point appears important for human myoblast transplantation efficiency,[27] as the NK-cell activity participates in death of the grafted cells.[28] One additional drawback of all of these models is the fact that they are all crossed into the *mdx* background and consequently the muscles will contain revertant fibers,[7] which can bias the readout based on the amount of dystrophin expressing fibers.[29]

In the present study, we describe the characterization of the newly developed *Rag2*$^{-}$*Il2rb*$^{-}$*Dmd*$^{-}$ immunodeficient mouse model, which lacks T, B, and NK cell activity.[16] The initial analyses were focused on body and muscle weights, showing that the compensatory hypertrophy described in the *mdx* model is also present in *Rag2*$^{-}$*Il2rb*$^{-}$*Dmd*$^{-}$ mice; measurements were very similar between the two strains (**Table 1**). Similar to the *mdx* mice, the specific muscle force and the resistance upon multiple lengthening contractions were both reduced in *Rag2*$^{-}$*Il2rb*$^{-}$*Dmd*$^{-}$ mice.

Positive confirmation of a dystrophic condition was also provided by the measurement of circulating creatine kinase, where both dystrophic models showed highly elevated levels caused by the membrane leakage induced by dystrophin deficiency.

A crucial point for assessing the regenerative capacity of human progenitors is to know precisely the natural kinetics of regeneration of the host. In both mouse models, the percentage of fibers with nonperipheral nuclei progressively increases over time (**Figure 1b**), as a result of at least one degeneration–regeneration cycle, and reached a plateau around 24 weeks, in agreement with the literature concerning the *mdx* model.[30] As for neonatal MyHC, most of the muscles of *Rag2*$^{-}$*Il2rb*$^{-}$*Dmd*$^{-}$ mice showed a higher percentage of fibers expressing neonatal MyHC, indicating that there was more active regeneration between 10 and 16 weeks of age compared with the *mdx* model. This means a 6-week long period of intensive regeneration, as opposed to a shorter 2-week long interval around the age of 3 weeks in the *mdx* mouse.[30] This wider window of intense regeneration in our new model could be due to the nature of the *Dmd*$^{mdx\text{-}\beta geo}$ allele that induces repeated cycles of muscle regeneration, or to the genetic background onto which this mouse strain is based: recent data have shown that the genetic background affects the endogenous muscle regeneration and therefore the phenotype severity.[31] However, we cannot rule out a potential effect of the immunodeficiency in the regeneration delay found in *Rag2*$^{-}$*Il2rb*$^{-}$*Dmd*$^{-}$ mice.

As several studies suggested a correlation between inflammatory response and fibrosis,[32,33] it could be expected that there would be less fibrosis in our new murine model deficient for both T and B cells, as it has been previously described in *mdx* mice lacking either T cells,[22] or both T and B cells.[34] Even if the infiltration of the residual inflammatory cell populations (i.e., macrophages

and neutrophils) correlates with degeneration/regeneration processes (**Supplementary Figure S2**), our quantification of the fibrotic deposition in the diaphragm muscle – a known hallmark for the progression of degenerative changes occurring in aged *mdx* mice[35] – revealed similar results in both dystrophic models (43% in the *mdx* and 37% in the *Rag2*$^{-}$*Il2rb*$^{-}$*Dmd*$^{-}$, $P < 0.05$). The complete absence in our model of both lymphocyte populations as well as NK cells, did not influence fibrosis; the slight difference observed between the two models is potentially due to the delay in the timing of muscle regeneration, which starts at 10 weeks of age in *Rag2*$^{-}$*Il2rb*$^{-}$*Dmd*$^{-}$ mice instead of 3 weeks in the *mdx*. Altogether, our results indicate that *Rag2*$^{-}$*Il2rb*$^{-}$*Dmd*$^{-}$ mice still have an important ongoing fibrotic process in certain muscles despite their lack of most inflammatory cells and suggest that B, T, and NK cells deficiencies do not seem to be involved in the development of fibrosis in the diaphragm in dystrophic mice; the slight difference observed between the two models is potentially due to the delay in the peak of muscle regeneration we discussed above.

At a molecular level, we confirmed the complete absence of dystrophin, and the associated dystrophin-glycoprotein complex, confirming that the *Dmd*$^{mdx\text{-}\beta geo}$ allele completely inhibits the production of truncated forms of dystrophin, contrary to what is classically observed for the *mdx* murine model (see[36] and **Figure 3a**). We also checked the presence of a fusion protein between dystrophin exons 1–63 and bGeo with an anti–n-terminal antibody, which did not reveal any positive signal (data not shown). The absence of revertant fibers will be a very important factor when evaluating the efficacy of therapeutic approaches since their presence will confound the quantification of the dystrophin^{+} fibers, as we would not know if they had reacquired the expression of dystrophin because of their "revertant" phenotype or due to the therapy that has been applied. An example of such problem goes back to the pioneer studies using bone marrow-derived myogenic cells, which turned out to be less efficient in restoring dystrophin than the natural reversion phenomena.[37]

Finally, we tested our *Rag2*$^{-}$*Il2rb*$^{-}$*Dmd*$^{-}$ model as a recipient for human cell transplantation by direct intramuscular injection. Primary human myoblasts integrated into the host muscle tissue and contributed to the generation of new muscle fibers expressing human proteins, where the only trigger was the natural existing dystrophic condition. Fibers that integrated human myoblasts were able to express and properly localize the human dystrophin and dystrophin-associated proteins at the sarcolemma. Moreover, transplanted cells could become part of the SC pool into the host tissue, as shown by the Pax7 immunostaining in **Figure 5**. Either mouse or human SCs were found between the sarcolemma and the basal lamina in human spectrin^{+} muscle fibers. In addition, human lamin A/C^{+} Pax7^{+} SCs were also found within mouse muscle fibers (data not shown), suggesting that human SCs recognize and interact with the mouse SC niche.

Previous studies on nondystrophic immunodeficient mice showed that without external stimuli (e.g., cryodamage, toxin injection, irradiation, and so on), the simple injection of human cells generated very few fibers, if any.[27,38] In our context, when cryodamage was applied higher numbers of spectrin^{+} fibers and human lamin A/C^{+} nuclei were obtained, although the difference was not statistically significant. These first results suggest that no additional damage is needed to assess the integration of human myoblasts in muscle fibers, and thus this mouse model can be used to analyze and study human cell behavior in a natural and physiologic dystrophic environment, although further experiments are required to confirm these results, and compare in terms of transplantation efficacy our model with the *scid/mdx* or the *nude/mdx*, which has been recently shown to allow the intramuscular injection of human cells into TAs after cryodamage.[39]

While this manuscript was finalized, a report described a new immunodeficient and dystrophic mouse strain (NSG-*mdx*^{4Cv}). However, even though its immunodeficient background is complete, the transplantation of allo and xenogeneic cells (from pig and dog) is only enhanced when the host muscle is preconditioned with irradiation and cardiotoxin.[40]

The *Rag2*$^{-}$*Il2rb*$^{-}$*Dmd*$^{-}$ mouse model carries a complete immunodeficient phenotype, lacking T- and B-cells, as well as the NK cell activity. In addition, it carries a new *Dmd* allele, which prevents the production of any truncated dystrophin. Both these features make this a superior model compared with the models that are presently available, and provide an appropriate model that do not require muscle conditioning to evaluate the graft efficiency of human myogenic stem cells, whether they are grafted intramuscularly or systemically, in order to assess and optimize human-targeted therapeutic strategies for muscular dystrophies.

Altogether, these data confirm that our *Rag2*$^{-}$*Il2rb*$^{-}$*Dmd*$^{-}$ model presents a clear dystrophic phenotype that is comparable with what is observed in the *mdx* mouse, and will be even better for stem cell assessment, thanks to its complete immunodeficient phenotype and prolonged window of regeneration.

MATERIALS AND METHODS

Animals. *Rag2*$^{-}$*Il2rb*$^{-}$*Dmd*$^{-}$ mice were generated by intercrossing *Rag2*$^{-}$*Il2rb*$^{-}$ mice[41] with *Dmd*$^{mdx\text{-}\beta geo}$ mice.[18] Mice bearing homozygous mutant alleles for all three genes were identified by genotyping DNA from tail clips (primer sequences available upon request). Two strains of dystrophic mice were used in this study: *Rag2*$^{-}$*Il2rb*$^{-}$*Dmd*$^{-}$, C57BL10ScSn-*Dmd*^{mdx}/J (*mdx*) and C57BL/6J (*wt*), the latter used as age-matched controls. All experiments were carried out in the specific pathogen-free animal facilities at the Faculty of Medicine of the University Pierre and Marie Curie (UPMC, Paris, France). Age-matched mice of each strain were sacrificed at different ages (4, 6, 8, 10, 12, 16, 24, and 43 weeks; at each time points $n \geq 6$). All experiments were performed in accordance with the legal regulations in France and European Union ethical guidelines for animal research.

Histology and immunohistochemistry. For histological and immunohistochemical analyses, TA, extensor digitorum longus, gastrocnemius, soleus and diaphragm muscles, were dissected, mounted in gum tragacanth (6% in water; Sigma-Aldrich, St. Louis, MO) on cork supports, frozen in isopentane precooled in liquid nitrogen, and stored at −80 °C until sectioning. The amount of total (endomysial plus perimysial) connective tissue was determined by Sirius red staining on 10-µm thick transverse cryosections of the tibialis anterior and diaphragm muscles.

For immunohistochemical analyses of muscle, cryosections were fixed with 4% PFA for 10 minutes at room temperature (RT), washed twice in PBS, and nonspecific binding was blocked in 1% BSA/PBS for 30 minutes at RT. Sections were then incubated with different primary antibodies: neonatal myosin heavy chain (neonatal MyHC) (rabbit polyclonal antibody, produced by GS Butler–Browne as previously described[42]), laminin (rabbit polyclonal, 1:400, Dako, Trappes, France), β-sarcoglycan (NCL-b-SARC, clone β Sarc/5B1, mouse monoclonal IgG1, 1:100, Novocastra, Newcastle upon Tyne, UK), dystrophin (rabbit polyclonal, 1:500, Thermo Fisher

Scientific, Fremont, CA). After incubation with the primary antibodies for 1 hour at RT or at 4 °C over night (ON), sections were washed twice for 10 minutes in PBS and the primary antibody staining was visualized with appropriate fluorochrome-conjugated secondary antibodies. The secondary antibodies used in this study were Alexa Fluor 488 goat anti-mouse IgG (1:500, Molecular Probes, Montluçon, France), Alexa Fluor 488 goat anti-rabbit (1:400, Molecular Probes) and Cy3 goat anti-rabbit (1:400, Jackson Immunoresearch, West Grove, PA). For analysis of muscle regeneration, transverse sections were used for double immunochemistry: immunostaining with laminin was performed ON and was followed by incubation with a Cy3-conjugated goat anti-rabbit secondary antibody. Afterwards, polyclonal antibody raised against neonatal MyHC was applied for 1h at RT and visualized with an Alexa Fluor 488 goat anti-rabbit antibody.

For the quantification of the immune infiltrate, cryosections were incubated 1 hour at RT with F4/80 (biotinilated rat monoclonal, clone A3-1, 1:50, AbD Serotec, Oxford, UK) or neutrophil Ly6g (rat monoclonal IgG2b, clone RB6-8C5, 1:50, Abcam, Cambridge, UK). The secondary antibodies used were: streptavidine conjugated Cy3 (1:400, Molecular Probes) and Cy3 goat anti-rat (1:300, Jackson Immunoresearch), respectively.

To visualize nuclei, the sections were mounted in medium (DakoCytomation Fluorescent mounting Medium, S3023) containing Hoechst (bis-benzimide, 0.0001% w/v, No. 33258; Sigma-Aldrich).

In order to identify injected human cells and fibers expressing human proteins, immunohistochemical analyses were performed on 5-µm thick transverse cryosections, incubating muscle sections with the following human-specific antibodies directed against: lamin A/C (clone JOL2, mouse monoclonal IgG1, 1:300, Abcam), and spectrin (NCL-Spec1, clone RBC2/3D5, mouse monoclonal IgG2b, 1:50, Novocastra). The secondary antibodies used were Cy3-conjugated goat anti-mouse IgG1 (1:500; Jackson ImmunoResearch), Alexa Fluor 488 goat anti-mouse (1:500; Molecular Probes), and Alexa Fluor 488 goat anti-mouse IgG2b (1:300; Molecular Probes).

To visualize the expression of dystrophin by human fibers, cryosections were first stained with spectrin (NCL-Spec1) and lamin A/C (clone 636, mouse monoclonal IgG2b, 1:400, Novocastra) to identify human fibers, and subsequently stained with human-specific MANDYS 102 (clone 7D2, mouse monoclonal IgG2a, 1:5, Developmental Studies Hybridoma Bank (DSHB), University of Iowa, Iowa City, IA), and MANDYS 106 (clone 2C6, mouse monoclonal IgG2a, 1:4, DSHB). To verify whether injected human cells also entered the satellite cell pool, sections were stained with an antibody against Pax7 (mouse monoclonal, IgG1, 1:20, DSHB). The secondary antibodies used were Alexa Fluor 488 goat anti-mouse IgG2b, Alexa Fluor 594 goat anti-mouse IgG2a (1:300, Molecular Probes), and Cy3-conjugated goat anti-mouse IgG1 (1:500; Jackson ImmunoResearch).

To verify the colocalization of dystrophin and dystrophin-associated proteins, serial cryosections were stained with lamin A/C (clone JOL2, mouse monoclonal IgG1, 1:300, Abcam), with dystrophin MANEX1216A (clone 5A4, mouse monoclonal IgG2a, 1:100, DSHB) or dystrophin MANDYS107 (clone 4H8, mouse monoclonal IgG2b, 1:100, DSHB), and with β-sarcoglycan (clone RO-17, mouse monoclonal IgG2b, undiluted, Santa Cruz) or β-dystroglycan (MANDAG2, clone 7D11, mouse monoclonal IgG1, 1:100, developed by Morris GE). The secondary antibodies used Alexa fluor 488 goat anti-mouse IgG1 (1:400, Molecular probes), Alexa fluor 488 goat anti-mouse IgG2a (1:400, Molecular probes) and Alexa fluor 594 goat anti-mouse IgG2b (1:400, Molecular probes).

Image acquisition and analysis. For histological analyses, the amount of fibrotic tissue was quantified from Sirius Red stained cryosections on at least three randomly selected fields from each muscle section. For each field, the area occupied by connective tissue was measured using the MetaMorph imaging system (Roper Scientific, Tucson, AZ) software and expressed as a percentage of the total muscle section area. For immunohistochemical analyses, montage images of the whole transverse section of the extensor digitorum longus and soleus muscles were acquired using the motorized stage of the Zeiss Imager.Z1 microscope (Carl Zeiss, Oberkochen, Germany) and digitalized using a CCD camera (Hamamatsu ORCA-ER; Shizuoka, Japan). For the TA and gastrocnemius, three digital pictures (10-fold magnification) were randomly acquired over the muscle section, using an Olympus BX60 microscope (Olympus Optical, Hamburg, Germany) and digitalized using a CCD camera (Photometrics CoolSNAP fx; Roper Scientific). Images of human nuclei and of fibers expressing human proteins within the injected muscles were acquired with a confocal FV-1000 microscope (Olympus) and digitalized with its dedicated software. All of the digital pictures were then analyzed using the MetaView image analysis system (Universal Imaging, Downington, PA).

Human myoblast culture and transplantation. Myoblasts isolated from the quadriceps muscle of a 5-day-old infant, isolated as already described,[43] were used in accordance with the French legislation on ethical rules. Cells were grown in Ham's F10 growth medium (Life Technologies, Saint Aubain, France) supplemented with 50 µg/ml of gentamycin (Life Technologies) and 20% fetal calf serum (Life Technologies) at 37 °C in a humid atmosphere containing 5% CO_2. At each passage, the number of divisions was calculated according to the formula: ln (N/n)/ln 2, where N is the number of cells counted and n is the number of cells initially plated. All experiments were performed using cell populations between 20 and 25 PDLs since isolation, in order to avoid any bias linked to proliferative ageing.

12-week-old *Rag2*$^{-}$*Il2rb*$^{-}$*Dmd*$^{-}$ mice were used as recipients for human cell transplantation. Mice were anesthetized with an intraperitoneal injection of ketamine hydrochloride (80 mg/kg) and xylazine (10 mg/kg) (Sigma-Aldrich) as described previously,[44] in accordance with the French legislation. In one group of animals, recipient TAs (n = 3) were exposed and subjected to three cycles of muscle freezing–thawing for 10 seconds each to induce severe muscle damage and trigger regeneration.[27] Immediately after cryodamage, human myoblasts (15-µl cell suspension containing 5×10^5 cells in PBS) were injected, using a 25-µl Hamilton syringe, in a single midpoint site along the longitudinal axis of the TA and the skin was then closed using a fine suture. In a second group of animals, undamaged TAs (n = 5) were injected using the same procedure. At 4 weeks after transplantation, mice were killed by cervical dislocation and TA muscles were collected as described above. Surgical procedures were performed in accordance with the legal regulations in France and European Union ethical guidelines for animal research.

CK assay. Blood was collected by orbital sinus bleeding using heparinized hematocrite tubes and centrifuged for 12 minutes at 12,000 rpm at 4 °C. Serum samples were stored at −80 °C prior to analysis, and CK activity was determined by the CK NAC-activated kit (Randox Laboratories, Antrim, UK) with the BioTek PowerWave 340 (BioTek UK, Bedfordshire, UK). The plot was created using JMP 10 software (SAS Institute, Cary, NC) to display a smoothing spline (cubic with lambda of 0.05).

Measurements of muscle contractile properties. Contractile properties of the TA muscles were evaluated by measuring the *in situ* isometric muscle contraction in response to nerve stimulation as described previously.[45] Mice were anesthetized using a pentobarbital solution (60 mg/kg intraperitoneally). The knee and foot were fixed with clamps and the distal tendon of the TA muscle to a lever arm of a servomotor system (305B, Dual-Mode Lever, Aurora, Canada). The sciatic nerve (proximally crushed) was stimulated by a bipolar silver electrode using supramaximal (10 V) square wave pulse of 0.1 ms duration. All isometric contraction measurements were made at an initial muscle length of L0 (length at which maximal tension was obtained during the twitch). Absolute maximal force was measured during isometric contractions in response to electrical stimulation (frequency of 100–150 Hz, train of stimulation of 500 ms). Specific maximal force was calculated by dividing absolute maximal force by muscle weight measured just after the force test. The *in situ* contraction-induced injury protocol for the TA muscle used in this study was similar to that described previously.[46] The sciatic nerve was stimulated for 700 ms (frequency of 125 Hz). An isometric contraction of the TA muscle was initiated during the first 500 ms. Then,

muscle lengthening (1.1 mm, about 10% Lf) at a velocity of 5.5 mm/s (about 0.5 Lf/s) was imposed during the last 200 ms. Ten lengthening contractions of the TA muscle were performed, each separated by a 60-second rest period. The "force deficit" after eccentric contraction-induced damage was determined by calculating the difference between the P0 measured 1 minute after the lengthening contractions and the P0 determined before lengthening contractions and was expressed as a percentage of P0 before damage.

Statistical analysis. Data are presented as the mean of the different animals ± SEM. All statistical analyses were carried out using GraphPad Prism (version 4.0b; GraphPad Software, San Diego, CA). All statistical analyses were performed using either the Student *t*-test, or the ANOVA one-way analysis of variance followed by the Newman–Keuls post-test. *P* values ≤0.05 were considered significant, see figure and table legends for more precise indications.

SUPPLEMENTARY MATERIAL

Figure S1. Quantification (a and b) of the chronology of regeneration in EDL and Soleus muscles of *Rag2–Il2rb–Dmd–* mice compared with mdx.

Figure S2. The number of neutrophils and macrophages was quantified in TA muscle sections of *Rag2–Il2rb–Dmd–* mice.

ACKNOWLEDGMENTS

The authors thank George Dickson and Alberto Malerba for help with the CK assay, and Odile Richard-LeGoff for help with mouse genotyping. The authors also thank Terry Partridge for fruitful discussions. This work was supported by the ANR In-A-Fib, the EU (Myoage contract number HEALTH-F2-2009-223576 from the 7th FP), the Association Française contre les Myopathies (AFM), DPP-NL, DIM Biothérapies from the Région Ile-de-France, Université Franco-Italienne, Fondation de l'Avenir (ET2-659). CAJV and JPD are supported by grants from the Institut Pasteur and the Inserm. The monoclonal antibodies developed by Morris GE were obtained from the Developmental Studies Hybridoma Bank developed under the auspices of the NICHD and maintained by The University of Iowa, Department of Biology, Iowa City, IA 52242". The authors declare no conflicts of interest.

REFERENCES

1. Mendell, JR, Shilling, C, Leslie, ND, Flanigan, KM, al-Dahhak, R, Gastier-Foster, J *et al.* (2012). Evidence-based path to newborn screening for Duchenne muscular dystrophy. *Ann Neurol* **71**: 304–313.
2. Matsuo, M (2002). Duchenne and Becker muscular dystrophy: from gene diagnosis to molecular therapy. *IUBMB Life* **53**: 147–152.
3. Decary, S, Hamida, CB, Mouly, V, Barbet, JP, Hentati, F and Butler-Browne, GS (2000). Shorter telomeres in dystrophic muscle consistent with extensive regeneration in young children. *Neuromuscul Disord* **10**: 113–120.
4. Willmann, R, Possekel, S, Dubach-Powell, J, Meier, T and Ruegg, MA (2009). Mammalian animal models for Duchenne muscular dystrophy. *Neuromuscul Disord* **19**: 241–249.
5. Bulfield, G, Siller, WG, Wight, PA and Moore, KJ (1984). X chromosome-linked muscular dystrophy (mdx) in the mouse. *Proc Natl Acad Sci USA* **81**: 1189–1192.
6. Sicinski, P, Geng, Y, Ryder-Cook, AS, Barnard, EA, Darlison, MG and Barnard, PJ (1989). The molecular basis of muscular dystrophy in the mdx mouse: a point mutation. *Science* **244**: 1578–1580.
7. Danko, I, Chapman, V and Wolff, JA (1992). The frequency of revertants in mdx mouse genetic models for Duchenne muscular dystrophy. *Pediatr Res* **32**: 128–131.
8. De Luca, A (2012). Pre-clinical drug tests in the mdx mouse as a model of dystrophinopathies: an overview. *Acta Myol* **31**: 40–47.
9. Trollet, C, Athanasopoulos, T, Popplewell, L, Malerba, A and Dickson, G (2009). Gene therapy for muscular dystrophy: current progress and future prospects. *Expert Opin Biol Ther* **9**: 849–866.
10. Negroni, E, Vallese, D, Vilquin, JT, Butler-Browne, G, Mouly, V and Trollet, C (2011). Current advances in cell therapy strategies for muscular dystrophies. *Expert Opin Biol Ther* **11**: 157–176.
11. Partridge, TA, Grounds, M and Sloper, JC (1978). Evidence of fusion between host and donor myoblasts in skeletal muscle grafts. *Nature* **273**: 306–308.
12. Flanagan, SP (1966). 'Nude', a new hairless gene with pleiotropic effects in the mouse. *Genet Res* **8**: 295–309.
13. Murphy, WJ, Durum, SK, Anver, MR, Ferris, DK, McVicar, DW, O'Shea, JJ *et al.* (1994). Induction of T cell differentiation and lymphomagenesis in the thymus of mice with severe combined immune deficiency (SCID). *J Immunol* **153**: 1004–1014.
14. Løvik, M (1995). The SCID (severe combined immunodeficiency) mouse–its biology and use in immunotoxicological research. *Arch Toxicol* (suppl. 17): 455–467.
15. Shinkai, Y, Rathbun, G, Lam, KP, Oltz, EM, Stewart, V, Mendelsohn, M *et al.* (1992). RAG-2-deficient mice lack mature lymphocytes owing to inability to initiate V(D)J rearrangement. *Cell* **68**: 855–867.
16. Kuwajima, S, Sato, T, Ishida, K, Tada, H, Tezuka, H and Ohteki, T (2006). Interleukin 15-dependent crosstalk between conventional and plasmacytoid dendritic cells is essential for CpG-induced immune activation. *Nat Immunol* **7**: 740–746.
17. Colucci, F, Soudais, C, Rosmaraki, E, Vanes, L, Tybulewicz, VL and Di Santo, JP (1999). Dissecting NK cell development using a novel alymphoid mouse model: investigating the role of the c-abl proto-oncogene in murine NK cell differentiation. *J Immunol* **162**: 2761–2765.
18. Wertz, K and Füchtbauer, EM (1998). Dmd(mdx-beta geo): a new allele for the mouse dystrophin gene. *Dev Dyn* **212**: 229–241.
19. Meng, J, Muntoni, F and Morgan, JE (2011). Stem cells to treat muscular dystrophies - where are we? *Neuromuscul Disord* **21**: 4–12.
20. Tedesco, FS and Cossu, G (2012). Stem cell therapies for muscle disorders. *Curr Opin Neurol* **25**: 597–603.
21. Morgan, JE, Pagel, CN, Sherratt, T and Partridge, TA (1993). Long-term persistence and migration of myogenic cells injected into pre-irradiated muscles of mdx mice. *J Neurol Sci* **115**: 191–200.
22. Morrison, J, Lu, QL, Pastoret, C, Partridge, T and Bou-Gharios, G (2000). T-cell-dependent fibrosis in the mdx dystrophic mouse. *Lab Invest* **80**: 881–891.
23. Torrente, Y, Belicchi, M, Sampaolesi, M, Pisati, F, Meregalli, M, D'Antona, G *et al.* (2004). Human circulating AC133(+) stem cells restore dystrophin expression and ameliorate function in dystrophic skeletal muscle. *J Clin Invest* **114**: 182–195.
24. Golumbek, PT, Keeling, RM and Connolly, AM (2007). RAG2 gene knockout in mice causes fatigue. *Muscle Nerve* **36**: 471–476.
25. Clark, EA, Shultz, LD and Pollack, SB (1981). Mutations in mice that influence natural killer (NK) cell activity. *Immunogenetics* **12**: 601–613.
26. Dorshkind, K, Pollack, SB, Bosma, MJ and Phillips, RA (1985). Natural killer (NK) cells are present in mice with severe combined immunodeficiency (scid). *J Immunol* **134**: 3798–3801.
27. Silva-Barbosa, SD, Butler-Browne, GS, Di Santo, JP and Mouly, V (2005). Comparative analysis of genetically engineered immunodeficient mouse strains as recipients for human myoblast transplantation. *Cell Transplant* **14**: 457–467.
28. Hodgetts, SI and Grounds, MD (2003). Irradiation of dystrophic host tissue prior to myoblast transfer therapy enhances initial (but not long-term) survival of donor myoblasts. *J Cell Sci* **116**(Pt 20): 4131–4146.
29. Arechavala-Gomeza, V, Kinali, M, Feng, L, Guglieri, M, Edge, G, Main, M *et al.* (2010). Revertant fibres and dystrophin traces in Duchenne muscular dystrophy: implication for clinical trials. *Neuromuscul Disord* **20**: 295–301.
30. Pastoret, C and Sebille, A (1995). mdx mice show progressive weakness and muscle deterioration with age. *J Neurol Sci* **129**: 97–105.
31. Fukada, S, Morikawa, D, Yamamoto, Y, Yoshida, T, Sumie, N, Yamaguchi, M *et al.* (2010). Genetic background affects properties of satellite cells and mdx phenotypes. *Am J Pathol* **176**: 2414–2424.
32. Andreetta, F, Bernasconi, P, Baggi, F, Ferro, P, Oliva, L, Arnoldi, E *et al.* (2006). Immunomodulation of TGF-beta 1 in mdx mouse inhibits connective tissue proliferation in diaphragm but increases inflammatory response: implications for antifibrotic therapy. *J Neuroimmunol* **175**: 77–86.
33. Madaro, L, Pelle, A, Nicoletti, C, Crupi, A, Marrocco, V, Bossi, G *et al.* (2012). PKC theta ablation improves healing in a mouse model of muscular dystrophy. *PLoS ONE* **7**: e31515.
34. Farini, A, Meregalli, M, Belicchi, M, Battistelli, M, Parolini, D, D'Antona, G *et al.* (2007). T and B lymphocyte depletion has a marked effect on the fibrosis of dystrophic skeletal muscles in the scid/mdx mouse. *J Pathol* **213**: 229–238.
35. Stedman, HH, Sweeney, HL, Shrager, JB, Maguire, HC, Panettieri, RA, Petrof, B *et al.* (1991). The mdx mouse diaphragm reproduces the degenerative changes of Duchenne muscular dystrophy. *Nature* **352**: 536–539.
36. Yokota, T, Lu, QL, Morgan, JE, Davies, KE, Fisher, R, Takeda, S *et al.* (2006). Expansion of revertant fibers in dystrophic mdx muscles reflects activity of muscle precursor cells and serves as an index of muscle regeneration. *J Cell Sci* **119**(Pt 13): 2679–2687.
37. Ferrari, G, Stornaiuolo, A and Mavilio, F (2001). Failure to correct murine muscular dystrophy. *Nature* **411**: 1014–1015.
38. Silva-Barbosa, SD, Butler-Browne, GS, de Mello, W, Riederer, I, Di Santo, JP, Savino, W *et al.* (2008). Human myoblast engraftment is improved in laminin-enriched microenvironment. *Transplantation* **85**: 566–575.
39. Meng, J, Adkin, CF, Xu, SW, Muntoni, F and Morgan, JE (2011). Contribution of human muscle-derived cells to skeletal muscle regeneration in dystrophic host mice. *PLoS ONE* **6**: e17454.
40. Arpke, RW, Darabi, R, Mader, TL, Zhang, Y, Toyama, A, Lonetree, CL *et al.* (2013). A New Immuno- Dystrophin-Deficient Model, the NSG-Mdx(4cv) Mouse, Provides Evidence for Functional Improvement Following Allogeneic Satellite Cell Transplantation. *Stem Cells* **31**: 1611–1620.
41. Vosshenrich, CA, Ranson, T, Samson, SI, Corcuff, E, Colucci, F, Rosmaraki, EE *et al.* (2005). Roles for common cytokine receptor gamma-chain-dependent cytokines in the generation, differentiation, and maturation of NK cell precursors and peripheral NK cells in vivo. *J Immunol* **174**: 1213–1221.
42. Butler-Browne, GS and Whalen, RG (1984). Myosin isozyme transitions occurring during the postnatal development of the rat soleus muscle. *Dev Biol* **102**: 324–334.
43. Decary, S, Mouly, V, Hamida, CB, Sautet, A, Barbet, JP and Butler-Browne, GS (1997). Replicative potential and telomere length in human skeletal muscle: implications for satellite cell-mediated gene therapy. *Hum Gene Ther* **8**: 1429–1438.
44. Negroni, E, Riederer, I, Chaouch, S, Belicchi, M, Razini, P, Di Santo, J *et al.* (2009). *In vivo* myogenic potential of human CD133+ muscle-derived stem cells: a quantitative study. *Mol Ther* **17**: 1771–1778.
45. Koo, T, Malerba, A, Athanasopoulos, T, Trollet, C, Boldrin, L, Ferry, A *et al.* (2011). Delivery of AAV2/9-microdystrophin genes incorporating helix 1 of the coiled-coil motif in the C-terminal domain of dystrophin improves muscle pathology and restores the level of a1-syntrophin and a-dystrobrevin in skeletal muscles of mdx mice. *Hum Gene Ther* **22**: 1379–1388.
46. Foster, H, Sharp, PS, Athanasopoulos, T, Trollet, C, Graham, IR, Foster, K *et al.* (2008). Codon and mRNA sequence optimization of microdystrophin transgenes improves expression and physiological outcome in dystrophic mdx mice following AAV2/8 gene transfer. *Mol Ther* **16**: 1825–1832.